Diffuse x-ray determination of local atomic order in a spin-glass alloy system

H. Bouchiat, E. Dartyge, P. Monod, and M. Lambert
Laboratoire de Physique des Solides, Université Paris Sud, 91405 Orsay, France*
(Received 27 May 1980)

In order to bring additional information pertinent to the so-called scaling laws for the magnetic properties of a spin-glass system, we have investigated the x-ray diffuse scattering of single crystals of *Ag*Mn alloys of 1, 3, 6, 8, 10, 15, 20, and 24 at.% Mn concentration quenched from 900 °C. Above 8% short-range order in the alloys manifests itself by the appearance of diffuse spots centered at $1\frac{1}{2}0$ and equivalent points in the fcc reciprocal space. The relative intensity of these diffuse spots increases with increasing concentrations up to 24 at.%. A detailed analysis has been undertaken of the possible atomic ordered structures compatible with our findings which are qualitatively similar to those investigated by Sato *et al.* on the *Cu*Mn system with neutrons. We show, in particular, that the structure DO_{22} can neither account for our *Ag*Mn system nor for the *Cu*Mn system for which it was advocated by Sato *et al.* We propose two possible models based on the structure $I4_1/amd$: one is essentially inhomogeneous in concentration and would imply the presence of microdomains of stoichiometry AgMn whose size and orientation are deduced from the observed shape and width of the diffuse spots; the other, more homogeneous one would imply periodic concentration modulation perpendicular to the (210) planes, as has already been proposed by De Fontaine and others for similar situations. A choice between these two models can be made in principle from the small-angle x-ray scattering data which have been obtained on the same samples. Surprisingly, our results show that for $2\times10^{-2} < 2\sin\theta/\lambda < 9\times10^{-2}$ Å^{-1} the scattered x-ray intensity is approximately independent of Mn concentration and corresponds to the Laue uniform background expected from a 6% disordered alloy. This finding tends to rule out the concentration wave hypothesis; however, a number of difficulties remain. The magnetic implication of the two models is briefly discussed in view of the known spin-glass parameters.

I. INTRODUCTION

Dilute alloys of magnetic atoms in a nonmagnetic metallic host (like *Cu*Mn or *Ag*Mn alloys) have a spin-glass[1] behavior at low temperatures. As the interaction between Mn localized spins is of the RKKY (Ruderman-Kittel-Kasuya-Yosida) type, its sign and amplitude depend on the relative manganese positions in the metal. In most cases they are supposed to be completely randomly distributed; this disorder is considered as one essential aspect of spin-glass and gives rise to the so-called scaling laws[2] for the concentration dependence of the alloy's properties. Such a hypothesis is quite natural and accepted for sufficiently dilute alloys (typically <1 at.%) but becomes more doubtful at higher concentrations. A precise knowledge of the position correlation and of the nature of the possible local order developing as a function of concentration is thus necessary for a more precise understanding of the magnetic properties of the alloy system in the paramagnetic and spin-glass state. The only experiments performed with that aim are neutron scattering measurements on *Cu*Mn alloys 15, 20, and 25 at.% by Sato *et al.*[3–5] and Ahmed and Hicks[6] at lower concentrations 2, 5, and 10 at.%. On the other hand, room-temperature measurements performed by Scheil and Watchel on copper and silver manganese alloys have shown an increase of the susceptibility of their samples between 10 and 30% by annealing at moderate temperature.[7,8] Modifications of the magnetic properties with the metallurgical state of Cu–25 at.% Mn alloy in the spin-glass temperature range have been observed by Beck[9] in a qualitative fashion.

The increase of susceptibility has been interpreted as local order developing with the annealing of the alloys. This local order is believed to decrease the number of the first-nearest-neighbor Mn atom pairs in favor of second-nearest-neighbor pairs. Indeed in *Cu* and *Ag*Mn alloys first-nearest-neighbor Mn pairs are believed to interact antiferromagnetically and second-nearest-neighbor pairs ferromagnetically.[10]

We have chosen to work on *Ag*Mn alloys somewhat less studied than *Cu*Mn as spin-glass alloys but which may be expected[7,8] to have the same kind of behavior as far as the short-range-order properties are concerned. However in contrast to *Cu*Mn, *Ag*Mn alloys are readily studied by x rays because of

the sizable difference between silver and manganese atomic numbers.

II. PREPARATION OF THE SAMPLES

The single-crystal samples have been prepared with the Bridgmann method.[11] The liquid melt of the alloys was slowly cooled in quartz tubes just under the fusion point of silver. (The tubes were moved in a temperature gradient for 48 h.) Then they were quenched in water and kept at room temperature. Single crystals (around 12 g) were prepared with concentrations of 1, 3, 6, 9, 11, 15, 20, and 24 at.% Mn. The concentrations were measured by x-ray microprobe analysis of the samples.[12] It was checked that the fluctuations of concentration were less than one percent (relative value) over the diameter of the sample (typically 1 cm). Susceptibility measurements at room temperature with a vibrating sample magnetometer were in overall agreement with the microanalysis results and susceptibility results of Ref. 13. We will be concerned here only by the results of the "as-quenched" samples, leaving the question of annealing effects to a future report.

III. EXPERIMENTAL SETUP

For the x-ray investigation we have cut the single crystals by electroerosion along a (100) plane, followed by etching with concentrated HNO_3 down to the appropriate thickness to be observed by transmission of the $K\alpha$ molybdenum radiation (typically 70 μm). A monochromatic beam was obtained with a graphite monochromator [a small amount of second harmonic ($\lambda/2$) was present for the highest voltage used]. Two recording techniques were used:

(a) The sample and the photographic films are kept in fixed positions: the principle of this experimental method is identical to that described in Ref. 14.

(b) Buerger precession: this apparatus can record a selected plane of the reciprocal lattice in undistorted form (Ref. 15). A number of such photographic plates have been taken, out of which a selection is made. We first discuss the position of the observed spots and next their relative intensity.

IV. RESULTS

The precession photographic plate displayed in Fig. 1 is from the Ag-24 at.% Mn single crystal. It is a record of a ($hk0$) reciprocal plane. One notes first the very intense overexposed Bragg spots corresponding to the face-centered-cubic lattice points 200 and 220. Furthermore diffuse spots are observed to be localized symmetrically around 110 positions of the

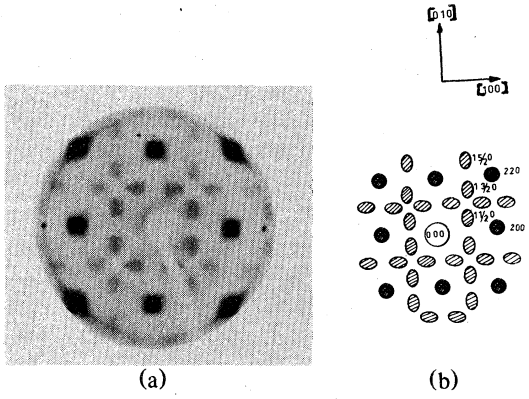

(a) (b)

FIG. 1. (a) Diffraction pattern of a Ag-24 at.% Mn single crystal. The radiation used is monochromatic Mo $K\alpha$, the second harmonic being eliminated. The Buerger precession apparatus is set up for a reciprocal ($hk0$) plane. (b) Indexing of the Bragg spots (●) and diffuse spots (●), which are recorded in an undistorted shape.

reciprocal lattice and centered on the $1 \pm \frac{1}{2}\,0$, $1 \pm \frac{3}{2}\,0$, and $\pm\frac{3}{2}10$ positions.

Indexing of these photographic plates taken with different orientations (see, for example, Figs. 2 and 3) shows that, besides the face-centered-cubic Bragg spots and diffuse streaks in agreement with thermal diffuse scattering observed for a pure silver crystal, diffuse spots are present for 24, 20, 15, 11, and 8 at.% Mn crystals at $1 \pm \frac{1}{2}\,0$, $\pm\frac{1}{2}01$, $0\,1 \pm \frac{1}{2}$, and all other positions deduced by fcc symmetry (see the

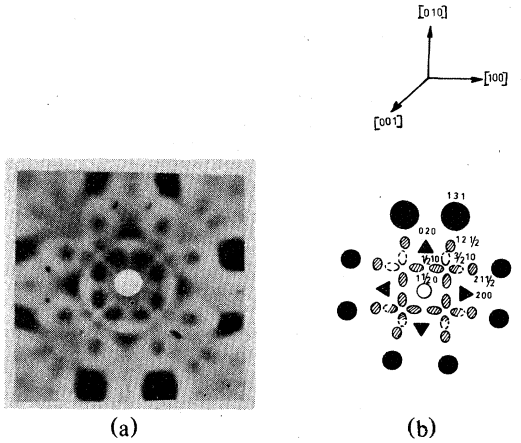

(a) (b)

FIG. 2. (a) Diffraction pattern of a Ag-20 at.% Mn single crystal: the plane photographic plate and the crystal are kept in a fixed orientation, with the incident x-ray beam along the [001] axis. The radiation used is monochromatic Mo $K\alpha$ (the second harmonic $\frac{1}{2}\lambda$ is not eliminated). (b) Indexing of the Bragg spots (●) and diffuse spots (●) seen in (a).

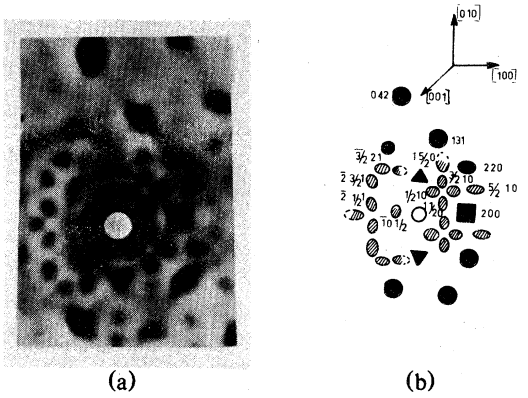

FIG. 3. (a) Diffraction pattern of a Ag-24 at.% Mn single crystal on a plane photographic plate. The radiation used is monochromatic Mo $K\alpha$ the second harmonic is eliminated. The crystal is kept in a fixed orientation in order to observe the diffuse spots centered on $\frac{1}{2}10$, $\frac{3}{2}10$, and $\frac{5}{2}10$ positions. (b) Indexing of the Bragg spots (●) and diffuse spots (⊘). Note the absence of diffuse intensity at 100 and 110 positions.

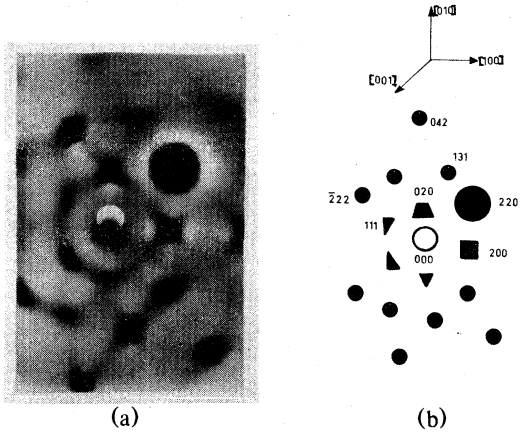

FIG. 5. (a) Diffraction pattern of a Ag-6 at.% Mn single crystal. The experimented conditions are the same as for the plate shown in Fig. 2. (b) Indexing of the visible Bragg spots. Diffuse spots are no longer visible. Only thermal scattering remains.

sketch Fig. 4). One can notice the absence of intensity at 100 and every fcc extinction position.

For all concentrations between 8 and 24 at.% the diffuse $1\frac{1}{2}0$ spots are more extended along the [010] axis than along the [100] and [001] axes; they appear less intense and more extended in all directions as the concentration is decreased from 24 to 8 at.%. Preliminary measurements from fixed plates show that the diffuse spots intensity seems to decrease somewhat more rapidly than linearly with the concentration. These diffuse spots are no longer visible below 6 at.% Mn (see Fig. 5) at room temperature. But they are slightly visible on a photographic plate made with the same sample at 80 K in order to eliminate partly the thermal diffuse scattering background. We have made a special microdensitometer investigation by which we can compare the integrated intensity of a $1\frac{3}{2}0$ diffuse spot, on the precession photograph (Fig. 6) taken with a 24 at.% Mn sample, to the total integrated intensity of a Bragg peak 200 on a 10-min photograph taken under the same conditions. When one takes into account the finite spatial resolution of the apparatus, this yields a total integrated intensity $3.5 \pm 0.5 \times 10^{-3}$ times lower for the diffuse spot than for the 200 Bragg peak (to be discussed below). By measuring (cf. Fig. 6) the spatial extension of a diffuse spot in reciprocal space [in

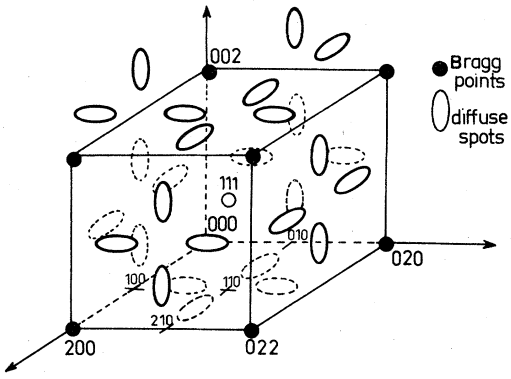

FIG. 4. Localization of the diffuse spots in the reciprocal space.

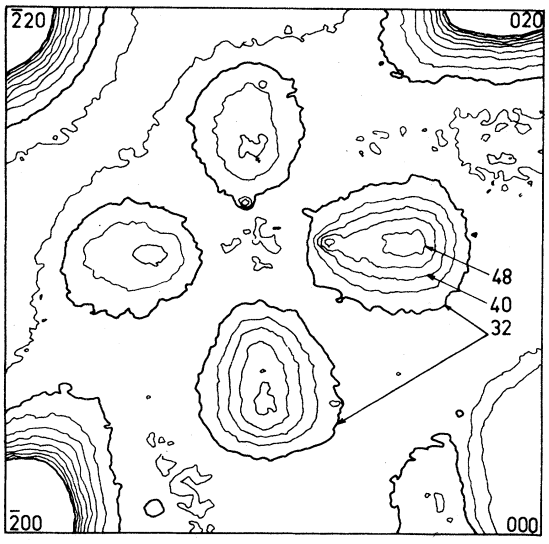

FIG. 6. Map of the diffuse isointensity lines in a (100) plane of the reciprocal space, obtained by microdensitometer investigation on the precession photo Fig. 1, of the Ag-24 at.% Mn sample.

reciprocal-lattice units (r.l.u.)], we find for a $1\frac{1}{2}0$ spot of the Ag-24 at.% Mn sample this extension to be: 0.30 ± 0.05 r.l.u. along the [010] direction and 0.20 ± 0.05 r.l.u. along the [100] and [001] directions. It is thus possible to give an order of magnitude of the atomic correlation length of the structure giving rise to this diffuse scattering: between 3 and 4 fcc cells along the [010] and between 5 and 6 fcc cells along the [001] and [100] axes.

The above experimental results can be compared to those obtained by neutron diffraction on *Cu*Mn alloys.[3–5] Diffuse peaks have been observed for 15, 20, and 25 at.% Mn alloys by Sato *et al.* along the $[h10]$ line in reciprocal space centered on the $\frac{1}{2}10$, $\frac{3}{2}10$, and $\frac{5}{2}10$ positions, in complete agreement with our observations. These *Cu*Mn diffuse peaks are more extended along the [100] direction than along the other directions, and they seem to decrease in intensity and broaden with decreasing concentration very much like our observation on the *Ag*Mn system.

The same kind of diffuse pattern has been also observed by electron diffraction in the disordered phases of Au_3Mn and Ni_4Mo alloys by Das and Okamoto.[16] We note that the latter alloys, contrary to *Cu*Mn and *Ag*Mn,[17] give rise to a completely ordered phase with definite stoichiometry.

V. DISCUSSION

The presence of diffuse spots at $\frac{1}{2}$ positions is characteristic of a short-range order whose period in one direction is twice the parameter of the initial fcc lattice. More precisely we want to discuss what structures in real space can account for the observed diffuse scattering. Sato *et al.*[4] interpret their observations on Cu-15–25 at.% Mn by the existence of small domains, having the completely ordered tetragonal $DO_{22}(I4/mmm)$ structure (Fig. 7). These domains have Cu_3Mn stoichiometry, and Cu and Mn atoms occupy the following positions in the tetragonal cell:

Mn: $000, \frac{1}{2}\frac{1}{2}\frac{1}{2}$,

Cu: $00\frac{1}{2}, 0\frac{1}{2}\frac{1}{4}, \frac{1}{2}0\frac{1}{4}, \frac{1}{2}\frac{1}{2}0, 0\frac{1}{2}\frac{3}{4}, \frac{1}{2}0\frac{3}{4}$.

The tetragonal direction is here [001]. The equivalent domains with [100] and [010] tetragonal directions must be taken into account when calculating the structure. However, in such a model we have checked that the amplitude factor *is the same* for the reciprocal-lattice point 100 as for the $1\frac{1}{2}0$ point even if the correlation length is only a few unit cells. The absence of intensity observed at the 100 point either by Sato *et al.*[3–5] on *Cu*Mn and in this present work on *Ag*Mn is in disagreement with such a model. Faced with this contradiction we have sought two different kinds of models which account for the positions of the observed spots and extinctions.

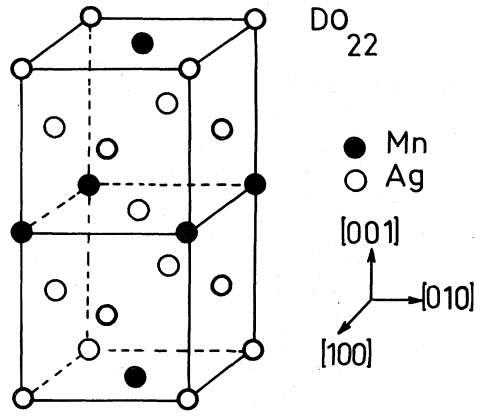

FIG. 7. Tetragonal cell of DO_{22} structure. The tetragonal axis being [001].

We first examined completely ordered structures with two different atoms. The only suitable one is associated with the $I4_1/amd$ group symmetry (Fig. 8). This structure has the stoichiometry AgMn; the tetragonal cell is obtained by juxtaposition of two face-centered-cubic cells, the respective position of Ag and Mn atoms being inverted in the two cells (in order to conserve the fcc extinctions at 100 and equivalent positions). Mn and Ag positions in a [001] direction tetragonal cell are: Mn: $000, \frac{1}{2}0\frac{1}{4}, \frac{1}{2}\frac{1}{2}\frac{1}{2}, 0\frac{1}{2}\frac{3}{4}$; and Ag: $\frac{1}{2}\frac{1}{2}0, 0\frac{1}{2}\frac{1}{4}, 00\frac{1}{2}, \frac{1}{2}0\frac{3}{4}$. This structure can also be described by the repeated juxtaposition of two Mn(021) planes and two Ag(021) planes. In that case, the atomic scattering factor at the fcc site $\vec{R}_i$ presents modulations of wave vector $\vec{k}_0$ and is given by

$$f(\vec{R}_i) = \tfrac{1}{2}(f_{Ag} + f_{Mn}) + (1/\sqrt{2})(f_{Mn} - f_{Ag})\cos(2\pi \vec{k}_0 \cdot \vec{R}_i + \tfrac{1}{4}\pi)$$

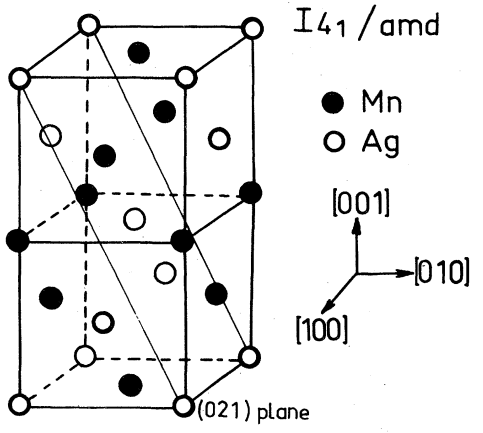

FIG. 8. Tetragonal cell of $I4_1/amd$ structure. The tetragonal axis being [001]. (For amplitude factors see Table I.) Notice the (021) plane containing only Ag atoms.

(f_{Ag} and f_{Mn} are the Ag and Mn atomic scattering factors). For one tetragonal axis, for example [001], there are four different possible choices for $\vec{k}_0$: $(0,1,\frac{1}{2})$, $(0,1,\frac{1}{2})$, $(1,0,\frac{1}{2})$, $(1,0,\frac{1}{2})$.

As the average concentration is only 24 at.% or less, this possible structure yields a description of the crystal in which a certain amount of the Mn atoms are included in such a $I4_1/amd$ 50 at.% stoichiometric structure domains (whose sizes are in agreement with the extension of diffuse spots in the reciprocal space). This implies important local inhomogeneities of concentration in the crystal.

As explained above, microdensitometer measurements of a diffuse $1\frac{1}{2}0$ spot on the 24 at.% sample make it possible to evaluate the proportion p of Mn atoms included in such domains. We do not make a large error (less than a few percent) when attributing to the Bragg 200 peak the intensity for the homogeneous disordered alloy: $4[cf_{Mn}+(1-c)f_{Ag}]^2$ per crystal atom (the volume of one reciprocal cubic cell being taken equal to unity). The measured ratio: r of the integrated intensity of a diffuse $1\frac{3}{2}0$ spot to a 200 Bragg peak is given by

$$r=\frac{\frac{2}{6}pc\,(f_{Ag}-f_{Mn})^2}{4[cf_{Mn}+(1-c)f_{Ag}]^2}$$

(angular dependence of scattering factors, Lorentz and polarization corrections are taken into account; for the $I4_1/amd$ structure factors see Table I). We find that the proportion p corresponds nearly to one-half of the Mn atoms.

Beside such a heterogeneous description, one can think of a homogeneous one in which each atom of the crystal is involved in a partially ordered domain having an average concentration equal to that of the crystal. To account for the observed $01\frac{1}{2}$ spots there must exist in these domains sinusoidal concentration fluctuations perpendicular to (021) planes. These fluctuations can be described by attributing to each crystal site $\vec{R}_i$ an atomic scattering factor equal to that of the average crystal: $cf_{Mn}+(1-c)f_{Ag}$ plus a $\vec{k}_0=01\frac{1}{2}$ wave-vector modulation $(\delta/\cos\phi)(f_{Mn}-f_{Ag})\cos(2\pi\vec{k}_0\cdot\vec{R}_i+\phi)$ with $0\leq\delta\leq c$. We have selected two characteristic cases corresponding to the respective choices of the phase factor $\phi=\frac{1}{4}\pi$ and 0.

a. $\phi=\frac{1}{4}\pi$. In this case the periodical concentration fluctuations can be described by the repeated juxtaposition of two (021) planes of average concentration $c+\delta$ and two (021) planes of average concentration $c-\delta$ with $\delta\leq c$ [Fig. 9(a)]. These fluctuations have the $I4_1/amd$ symmetry [the $I4_1/amd$ *Ag*Mn structure described above (Fig. 8) corresponds to $c=\delta=50$ at.%].

b. $\phi=0$. A domain with such concentration modulations can be described by the repeated juxtaposition of (021) planes with respective average con-

TABLE I. Calculated structure factors: $S(hkl)$ and $10\frac{1}{2}$ intensities for DO_{22}, $I4_1/amd$, and wave models.

Model / hkl[a]	DO_{22} stoichiometry Ag_3Mn (Fig. 7) $S(hkl)$	$I4_1/amd$ stoichiometry AgMn (Fig. 8) $S(hkl)$	Sinusoidal concentration modulations [Fig. 9(a)] $\phi=\frac{1}{4}\pi$ $S(hkl)$	Sinusoidal concentration modulations [Fig. 9(b)] $\phi=0$ $S(hkl)$
001	$2(f_{Ag}-f_{Mn})$	0	0	0
100				
010	0	0	0	0
110				
$00\frac{1}{2}$	0	0	0	0
$10\frac{1}{2}$	$2(f_{ag}-f_{Mn})$	$2(f_{Ag}-f_{Mn})(1\pm i)$	$4\delta(f_{Ag}-f_{Mn})(1\pm i)$	$4\delta(f_{Ag}-f_{Mn})$
$01\frac{1}{2}$				
I/at. for $1\frac{1}{2}0$[b]		$\frac{2}{6}pc\,(f_{Ag}-f_{Mn})^2$ [c]	$\frac{2}{3}\delta^2(f_{Ag}-f_{Mn})^2$ [d]	$\frac{1}{3}\delta^2(f_{Ag}-f_{Mn})^2$ [d]

[a]Structure factor for one tetragonal cell with tetragonal axis along the cubic [001] axis, calculated for the following hkl reciprocal cubic lattice points: $S(hkl)$.

[b]Integrated intensity of a diffuse spot per crystal atom. The three possible directions of tetragonal directions are taken into account. The volume of one reciprocal cell is taken equal to unity.

[c]p being the proportion of atoms included in $I4_1/amd$ microdomains.

[d]If we admit that all the Mn atoms are included in such concentration waves.

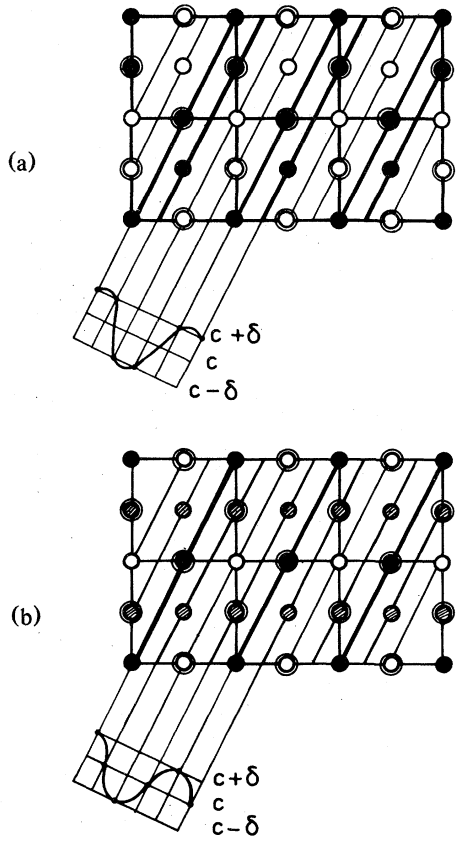

FIG. 9. Projection on a (100) plane of the atomic arrangement in a $1\frac{1}{2}0$ concentration wave: (a) keeping the $I4_1/amd$ symmetry ● points of average concentration $c+\delta$ (zeroth layer); ◉ points of average concentration $c+\delta$ ($\frac{1}{2}$ layer); ○ points of average concentration $c-\delta$ (zeroth layer); and ◎ points of average concentration $c-\delta$ ($\frac{1}{2}$ layer). (b) Concentration wave having a symmetry intermediate between DO_{22} and $I4_1/amd$ ● ◉ points of average concentration $c+\delta$ (at zero and $\frac{1}{2}$ layer, respectively); ⊘◉ points of average concentration c; and ○◎ points of average concentration $c-\delta$. (For amplitude factors see Table I.)

centrations $c-\delta$, c, $c+\delta$, c [Fig. 9(b)]. Such a description with $\delta=c$ (i.e., planes with $0,c,2c,c$ variation) has been used by Das *et al.*[16] and De Fontaine[18] for short-range order in quenched Ni_4Mo alloys. It does not have the symmetry I_{4_1}/amd, and presents some similarities with the DO_{22} structure which can be described in terms of nonsinusoidal atomic factor modulations. (That is in the Ag_3Mn stoichiometric case, the repeated juxtaposition of three Ag planes and one Mn plane.) For all these sinusoidal concentration modulations there is no diffuse intensity at 100 and equivalent points (for amplitude factors and the intensity of diffuse spots see Table I).

In all cases the elongated shape of the diffuse $1\frac{1}{2}0$ spots in the [010] direction must be explained by a domain size less extended in the [010] direction than in the others. It may be noticed that the descriptions (given in Fig. 9) are coherent only if statistical concentration fluctuations in a domain are small, compared to δ. If N is the number of atoms in a domain that implies

$$\delta \gg \sqrt{c/N} \ .$$

If we admit that all the atoms participating to the diffuse scattering are involved in such concentration waves, it is possible from the measured intensity value of a $1\frac{1}{2}0$ spot, to evaluate δ. For the Ag-24 at.% Mn sample δ was found to be roughly equal to c. For the same sample the number of atoms in a domain is estimated around $N=300$. $\sqrt{c/N}=3\times10^{-2}$ which is indeed small compared to c. This criterion is barely satisfied as the concentration decreases below 10 at.%. We further refer to these models a and b as the homogeneous or "wave model."

All these structures can be described in terms of the Warren short-range-order parameters[19]

$$\alpha(\vec{R}_i)=1-P(\vec{R}_i)/(1-c) \ ,$$

where $P(\vec{R}_i)$ is the probability to have an Ag atom at the site $\vec{R}_i$ if there is an Mn atom at the origin. In the case of a completely disordered alloy $\alpha(\vec{R}_i)=0$ for all $\vec{R}_i\neq0$. In an alloy where a $\vec{k}_0$ wave-vector-concentration wave is taking place

$$\alpha(\vec{R}_i)=(\delta^2/2\cos^2\phi)\cos2\pi(\vec{k}_0\cdot\vec{R}_i)$$

(assuming an infinite correlation length).

If the sums $\sum_1$ and $\sum_2$ are running, respectively, over the first- and second-neighbors $\vec{R}_i$ positions

$$\alpha_1=\tfrac{1}{12}\sum_1\alpha(\vec{R}_i)=-\frac{\delta^2}{6c(1-c)\cos^2\phi} \ ,$$

$$\alpha_2=\tfrac{1}{6}\sum_2\alpha(\vec{R}_i)=\frac{\delta^2}{6c(1-c)\cos^2\phi} \ .$$

As a matter of numerical example, we find for the case a ($\phi=\frac{1}{4}\pi$, $\delta=c=0.24$)

$$\alpha_1=-\alpha_2=-0.11 \ .$$

It is important to note that all these descriptions of domains whose Mn concentration is equal to the average concentration of the crystal yield a negative value for α_1 and a positive value for α_2 independent of the choice of the phase factor, the modulation amplitude δ, and the atomic correlation length. α_1 and α_2 are related to the numbers n_1 and n_2 of Ag first- and second-nearest neighbors around an Mn atom by the relations

$$\alpha_1=1-n_1/12(1-c), \quad \alpha_2=1-n_2/6(1-c) \ .$$

In the case $c=0.24$ the above values of α_1 and α_2

yield the number of Mn first- and second-nearest neighbors around an Mn atom, respectively, equal to

$$12 - n_1 = 1.9, \quad \text{Mn first neighbors} ,$$

$$6 - n_2 = 2, \quad \text{Mn second neighbors} ,$$

In the totally disordered homogeneous state these numbers are, respectively,

$$12 - n_1(\text{random}) = 2.9, \quad \text{Mn first neighbors} ,$$

$$6 - n_2(\text{random}) = 1.5, \quad \text{Mn second neighbors} .$$

We remark that a perfectly ordered $I4_1/amd$ structure corresponds to

$$12 - n_1(I4_1/amd) = 4, \quad \text{Mn first neighbors} ,$$

$$6 - n_2(I4_1/amd) = 4, \quad \text{Mn second neighbors} .$$

Thus an Mn atom included in such $I4_1/amd$ domain in a less than 25 at.% average concentration sample has more Mn first- and second-nearest neighbors than in the totally disordered homogeneous state.

VI. SMALL-ANGLE-SCATTERING RESULTS

Small-angle x-ray-scattering measurements were also performed on the different samples. The principles and experimental device of the experiments are given in Ref. 20. The intensity diffracted ΔI in a given solid angle $\Delta\omega$ was measured by a scintillation detector. Thus we obtained quantitative information about the absolute intensity diffracted in the reciprocal space region corresponding to $2\times10^{-2} < s = 2\sin\theta/\lambda < 9\times10^{-2}$ Å^{-1} (θ being the scattering angle). A typical set of measurements on pure Ag and Ag-20 at.% Mn are presented in Fig. 10(a).

In a completely disordered alloy we expect the small-angle-scattering power to grow with the concentration as the Laue intensity $I_L = c(1-c)(f_{Ag} - f_{Mn})^2$ (that is 77 e/at. for $c = 20$ at.% and must be added to the theoretical scattering power of silver: 15 e/at. as we know that there are no size effects in *Ag*Mn alloys). Figure 10(b) shows that $\Delta I/\Delta\omega$ (measured for $s = 8\times10^{-2}$ Å^{-1}) is nearly independent of the Mn concentration. How can the different local order descriptions exposed above, be consistent with this apparent absence of disorder observed in the small-angle region?

A. Description in terms of $I4_1/amd$ *Ag*Mn microdomains

If we admit that a large proportion of Mn atoms are included in ordered microdomains, the small-angle scattered intensity is expected to be much less than I_L calculated for complete disorder (except at angles inferior to the smallest angles of our investigation, where the microdomains scatter independently). That prediction of reduction of intensity is in qualitative agreement with the measurements. However, in the case of 24-at.% alloys a discrepancy arises between large-angle- and small-angle-scattering measurements, since with large-angle-scattering measurements we find that only half of the Mn atoms are included in the microdomains where as nearly 80% Mn atoms are found by small-angle scattering. But we certainly underestimated the integration of a diffuse spot by the microdensitometer measurements because of the slight overlap of the next two diffuse spots.

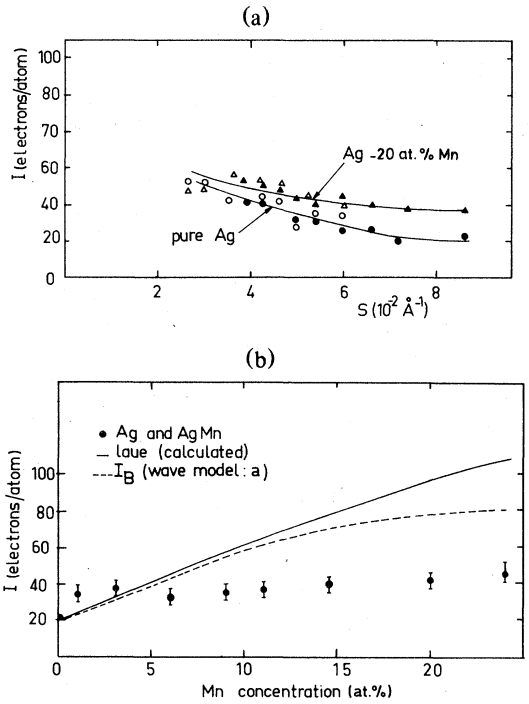

FIG. 10. (a) Comparison of intensity diffracted by an Ag sample (circles) and a 20 at.% Mn, *Ag*Mn sample (triangles). Two different experimental apparatus were used: Δ, ●: experiment performed with Mo $K\alpha$ radiation; and Δ, ○: experiment performed with Cu $K\alpha$ radiation. (b) Scattered intensity at $s = 8\times10^{-2}$ Å^{-1} vs Mn concentration. Continuous line: scattered intensity for a completely disordered alloy (Laue scattering power added to the experimental scattering power of silver). Dotted line homogeneous concentration wave model calculated for case a with $\delta = c$.

B. Concentration wave model

In such domains [Figs. 9(a) and 9(b)] there are no atomic correlations inside (120) planes. This remaining disorder should give rise to an important diffuse scattering background, I_B, observable in the small-angle region. If I_d is the integrated intensity of one

diffuse spot (see Table I) $\frac{3}{2}I_d$ is the diffuse intensity integrated over one reciprocal cell. The value of I_B obtained for $\delta = c$ is: case a; $I_B = I_L - \frac{3}{2}I_d = c(1 - 2c)(f_{Ag} - f_{Mn})^2$ per crystal atom and case b; $I_B = I_L - \frac{3}{2}I_d = c(1 - 3/2c)(f_{Ag} - f_{Mn})^2$ per crystal atom for the two choices of phase given in the discussion. These values for the 20 at.% sample are 58 and 68 *e*/at. respectively, and must be added to the diffuse scattering power of silver. So, these "concentration wave" models without supplementary atomic correlations imply the presence of a diffuse scattering background two times larger than that observed in our small-angle-scattering experiments. This observed low scattering power, can only be explained by a heterogeneous description in microdomains having locally a 50 at.% Mn concentration and involving $1\frac{1}{2}0$ concentration waves which can correspond to the $I4_1/amd$ structure but also to any other choice of phase factor.

VII. CONCLUSION: MAGNETIC IMPLICATIONS

A description in terms of DO_{22} ordered microdomains cannot account for the diffuse scattering pattern of *Ag*Mn and *Cu*Mn alloys. Among the possible heterogeneous descriptions of local order in terms of 50 at.% Mn concentration microdomains and homogeneous descriptions in terms of concentration modulations (which both agree qualitatively with the observed diffuse pattern) only the first are in agreement with the quantitative complementary information given by small-angle-scattering measurements.

It is important to note that, contrary to the DO_{22} structure, the $I4_1/amd$ structure does not eliminate the first-neighbor Mn pairs. So, at present it is still difficult to state what kind of magnetic order such an observed atomic local order implies. Assuming for the first and second manganese neighbor pairs antiferromagnetic and ferromagnetic interactions, it is tempting to explain the increase of the paramagnetic susceptibility as a consequence of the increase of the atomic local order in the framework of the homogeneous descriptions given above. Indeed in these descriptions the local order tends to decrease the number of first-neighbor pairs in favor of second-neighbor ones. This is not true for the heterogeneous description in terms of stoichiometric *Ag*Mn $I4_1/amd$ domains, where both α_1 and α_2 are positive inside the domains. Concerning the low-temperature magnetic behavior it is clear that the $I4_1/amd$ structure yields perfect antiferromagnetism (Fig. 11) contrarily to the DO_{22} structure which yields perfect ferromagnetism by eliminating all the first-neighbor Mn pairs. If one attributes to a $I4_1/amd$ microdomain containing n^3 Mn atoms a resulting (surface) magnetic moment proportional to n^2 one can expect an increase of remanent magnetization with the number of such domains (the average size of domains remaining the same), and on the other hand one expects a decrease of remanent magnetization with an increase of the average size of ordered domains the number of atoms included in the domains remaining the same.

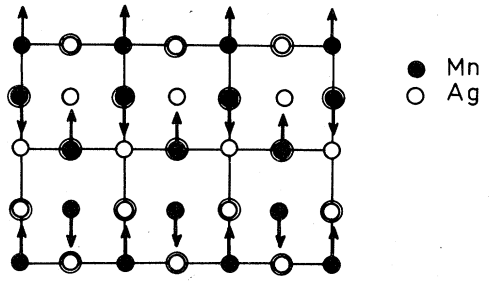

FIG. 11. Projection on a (100) plane of the lowest-energy configuration of Mn spins for the $I4_1/amd$ structure. (First- and second-neighbor magnetic interactions are taken into account.) The symbols used for different layers are the same as in Fig. 9.

Magnetic measurements are in progress in relation to the x-ray experiments in order to try to decide what kind of magnetic behavior modifications are really connected with the increase of local order which should be obtained by annealing the samples.

ACKNOWLEDGMENTS

We thank A. Guinier for helpful discussions. We also thank H. Bizouard, M. Lecoeuvre, M. Godard, and L. Deschamps for technical help.

---

*Laboratoire associé au CNRS.

[1]P. J. Ford and J. A. Mydosh, Phys. Rev. B 14, 2057 (1976).

[2]J. Souletie and R. Tournier, J. Low Temp. Phys. 1, 95 (1969).

[3]H. Sato, S. A. Werner, and R. Kikuchi, J. Phys. 35, 23 (1974).

[4]H. Sato, S. A. Werner, and M. Yessik, in *Magnetism and Magnetic Materials—1971,* edited by C. D. Graham, Jr., and J. J. Rhyne, AIP Conf. Proc. No. 5 (AIP, New York, 1972), p. 509; H. Sato, S. A. Werner, and M. Yessik, in *Causality and Physical Theories—1973,* edited by W. B. Rolnick, AIP Conf. Proc. No. 16 (AIP, New York, 1974), p. 679.

[5]Electron diffraction measurements on Cu-25 at.% Mn ap-

peared to be in complete disagreement with the neutron studies: H. Warlimont, K. Bernecker, and R. Lück, Z. Mettallkde. 62, 816 (1971). But it was further established that their observations were due to the presence of Cu_2O on the samples. [H. Sato, S. A. Werner, and M. Yessik, Z. Mettallkde. 64, 427 (1973).]

[6]N. Ahmed and T. J. Hicks, Solid State Commun. 15, 415 (1974).

[7]E. Scheil and E. Wachtel, Z. Mettallkde. 49, 464 (1958).

[8]E. Scheil and E. Wachtel, Z. Mettallkde. 48, 571 (1957).

[9]P. A. Beck, Prog. Mater. Sci. 23, 1 (1978).

[10]B. D. Rainford, J. Magn. Magn. Mater. 14, 197 (1979).

[11]J. P. Chapelle (private communication).

[12]They were 20% lower than the nominal concentrations because of the sublimation of a certain manganese amount.

[13]D. P. Morris and I. Williams, Proc. Phys. Soc. London 73, 422 (1959).

[14]R. Comès, M. Lambert, and H. Launois, Phys. Rev. B 8, 571 (1973).

[15]M. J. Buerger, *X-Ray Crystallography* (Wiley, New York 1958).

[16]S. K. Das, P. R. Okamoto, P. M. Fisher, and G. Thomas, Acta Metall. 21, 920 (1973).

[17]W. B. Pearson, *A Handbook of Lattice Spacings and Structures* (Pergamon, New York, 1956); P. R. Okamoto and G. Thomas, Acta Metall. 19, 825 (1971).

[18]D. De Fontaine, Solid State Phys. 34, 74 (1979); Acta Metall. 23, 560 (1975).

[19]A. Guinier, *Théorie et Technique de la Radiocristallographie* (Dunod, Paris, 1956).

[20]A. M. Levelut, M. Lambert, and A. Guinier, C. R. Acad. Sci. 255, 319 (1962).

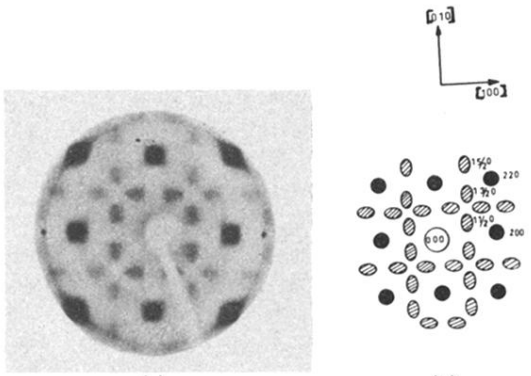

(a) (b)

FIG. 1. (a) Diffraction pattern of a Ag-24 at.% Mn single crystal. The radiation used is monochromatic Mo $K\alpha$, the second harmonic being eliminated. The Buerger precession apparatus is set up for a reciprocal ($hk0$) plane. (b) Indexing of the Bragg spots (●) and diffuse spots (⬬), which are recorded in an undistorted shape.

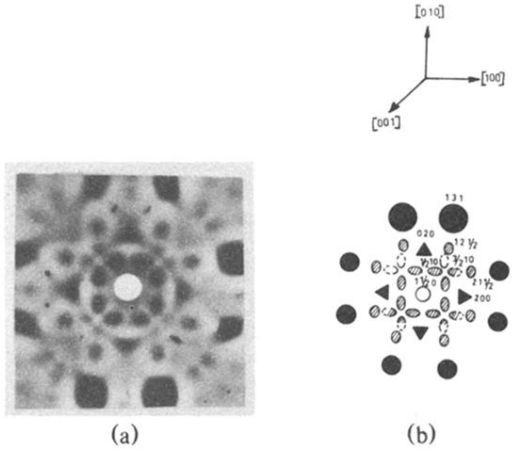

FIG. 2. (a) Diffraction pattern of a Ag-20 at.% Mn single crystal: the plane photographic plate and the crystal are kept in a fixed orientation, with the incident x-ray beam along the [001] axis. The radiation used is monochromatic Mo $K\alpha$ (the second harmonic $\frac{1}{2}\lambda$ is not eliminated). (b) Indexing of the Bragg spots (●) and diffuse spots (⬬) seen in (a).

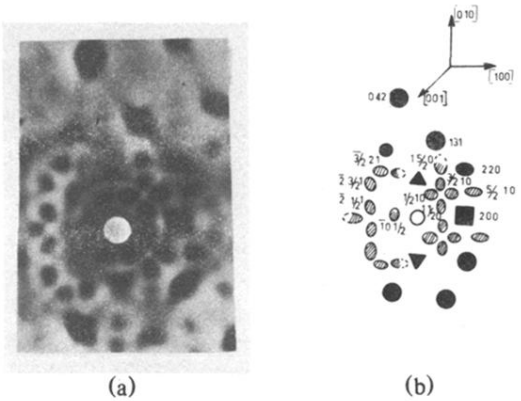

(a) (b)

FIG. 3. (a) Diffraction pattern of a Ag-24 at.% Mn single crystal on a plane photographic plate. The radiation used is monochromatic Mo $K\alpha$ the second harmonic is eliminated. The crystal is kept in a fixed orientation in order to observe the diffuse spots centered on $\frac{1}{2}10$, $\frac{3}{2}10$, and $\frac{5}{2}10$ positions. (b) Indexing of the Bragg spots (●) and diffuse spots (⊘). Note the absence of diffuse intensity at 100 and 110 positions.

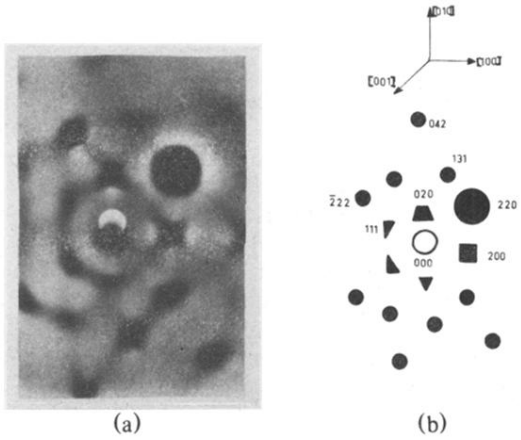

(a) (b)

FIG. 5. (a) Diffraction pattern of a Ag-6 at.% Mn single crystal. The experimented conditions are the same as for the plate shown in Fig. 2. (b) Indexing of the visible Bragg spots. Diffuse spots are no longer visible. Only thermal scattering remains.